FERMILAB-TM-2741-AD-APC

Studies of Beam Intensity Effects in Fermilab Booster Synchrotron

Part II: Beam Emittance Evolution

Vladimir Shiltsev, Jeff Eldred, Valery Lebedev, Kiyomi Seiya

Fermi National Accelerator Laboratory, PO Box 500, Batavia, IL 60510, USA

Abstract

Detrimental beam dynamics effects limit performance of high intensity rapid cycling synchrotrons (RCS) such as the 8 GeV Fermilab Booster. Here we report the results of comprehensive studies of various beam intensity dependent effects in the Booster. In the previous publication [1] we presented the dependencies of the Booster beam intensity losses on the total number of protons per pulse and on key operational parameters such as the machine tunes and chromaticities. Here we discuss two methods of the Booster beam emittance measurements (the multi-wires proportional chambers and the ionization profile monitors), analyze the intensity dependent emittance growth effects and discuss the ultimate performance of the machine now and after foreseen and proposed upgrades.

PACS numbers: 29.20.D-, 29.20.Lq, 29.27.Bd, 29.27.Fh

1. BOOSTER BEAM EMITTANCE DIAGNOSTICS

Brief description, main parameters and the intensity related effect on the transmission of the Fermilab Booster - a 474.2 m circumference, alternating-gradient, rapid-cycling synchrotron (RCS) – can be found in our previous paper [1]. Here we present results of the Booster beam emittance studies carried out as part of the Summer 2019 Booster Studies program [2].

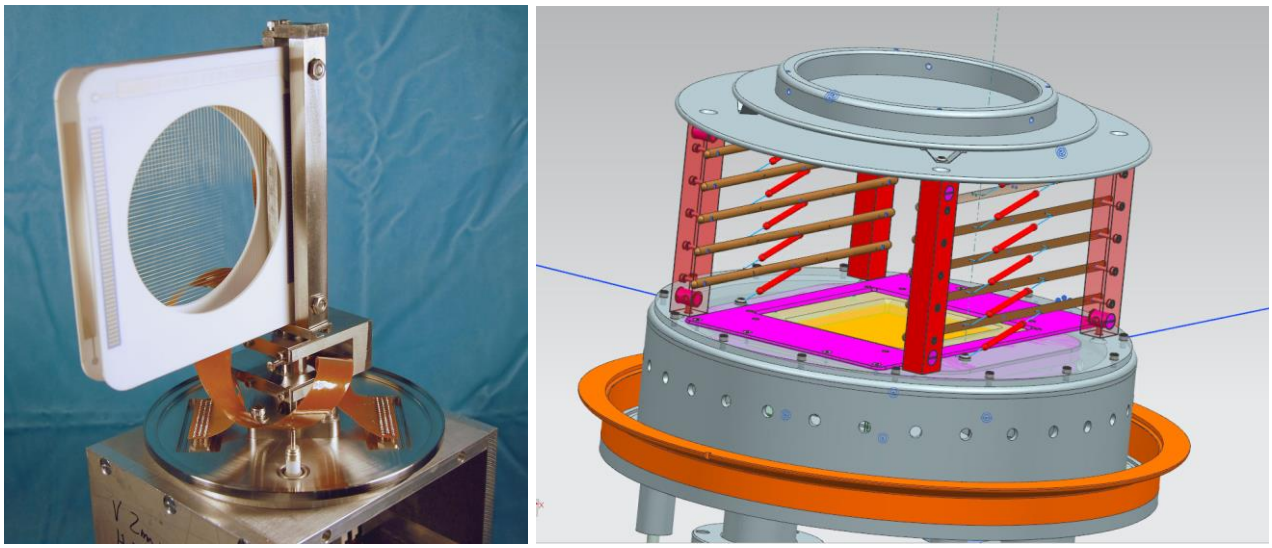

Figure 1: Booster beam emittance diagnostics: (left) multi-wires; (ionization) ionization profile monitor.

In the Booster, there are two types of instruments to measure beam sizes and therefore, transverse emittances – the multi-wires (MWs) and the ionization profile monitors (IPMs) – see Fig.1. Vertical and horizontal MWs are installed in the extraction beam line and therefore can measure only the emittances of the extracted Booster beam. There are 48 wires in each instrument, spaced by 1 mm. The focusing optics function at the MW location are β_x=16.2m, β_y=25.9m and D_x=-1.65m. Measured beam emittances at extraction exhibit strong dependence on the total proton intensity N_p, as shown in Fig. 2. Statistical rms error of the MW emittance measurement is about 0.05 mm mrad.

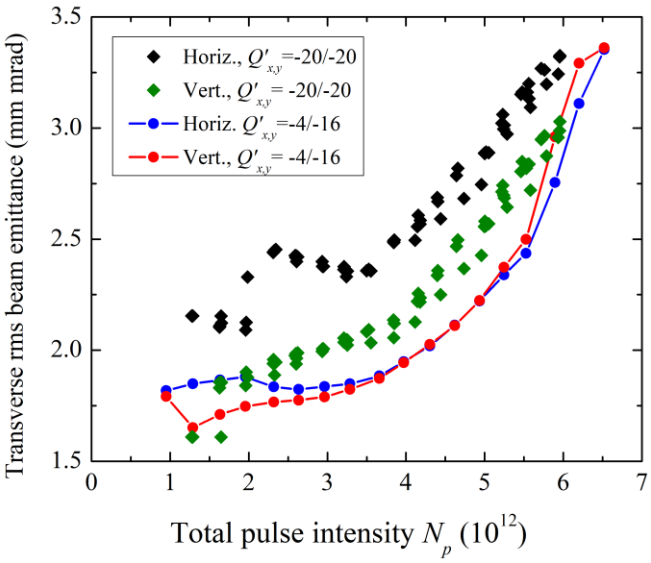

Figure 2: Booster beam emittance at extraction vs the total proton intensity.

Two IPMs – vertical and horizontal, are installed in the location with β_x=6.0m, β_y=20.3m and D_x=1.8m. In the IPM – see Fig.1 a) - proton beam goes through a 103 mm high HV cage. The maximum voltage on the upper plate is +24 kV, the electric field uniformity is arranged by six-stage voltage divider bars. Secondary ions, produced in the acts of ionization of the residual gas by the proton beam, are accelerated toward 80×100 mm^2 micro-channel plate (MCP, shown in gold). The MCP voltage, typically about 600V, allows to control the strength of the signal. Electrons, out-coming from the MCP, proceed for another 7.5 mm to an array of parallel thin anode strips at +100V spaced 1.5 mm apart (not shown) where they are collected and amplified for further processing. IPMs report the average rms beam sizes (determined by the Gaussian fits of the profiles) every turn – see, e.g., Fig.3 for a typical data for a cycle with operational beam intensity, tunes and chromaticities. The IPM outcomes are dependent on the proton beam intensity as the

proton space charge fields lead to expansion of the transverse distribution of the secondary ion collected at the MCP, and, therefore, a correction is needed to determine the actual rms beam sizes.

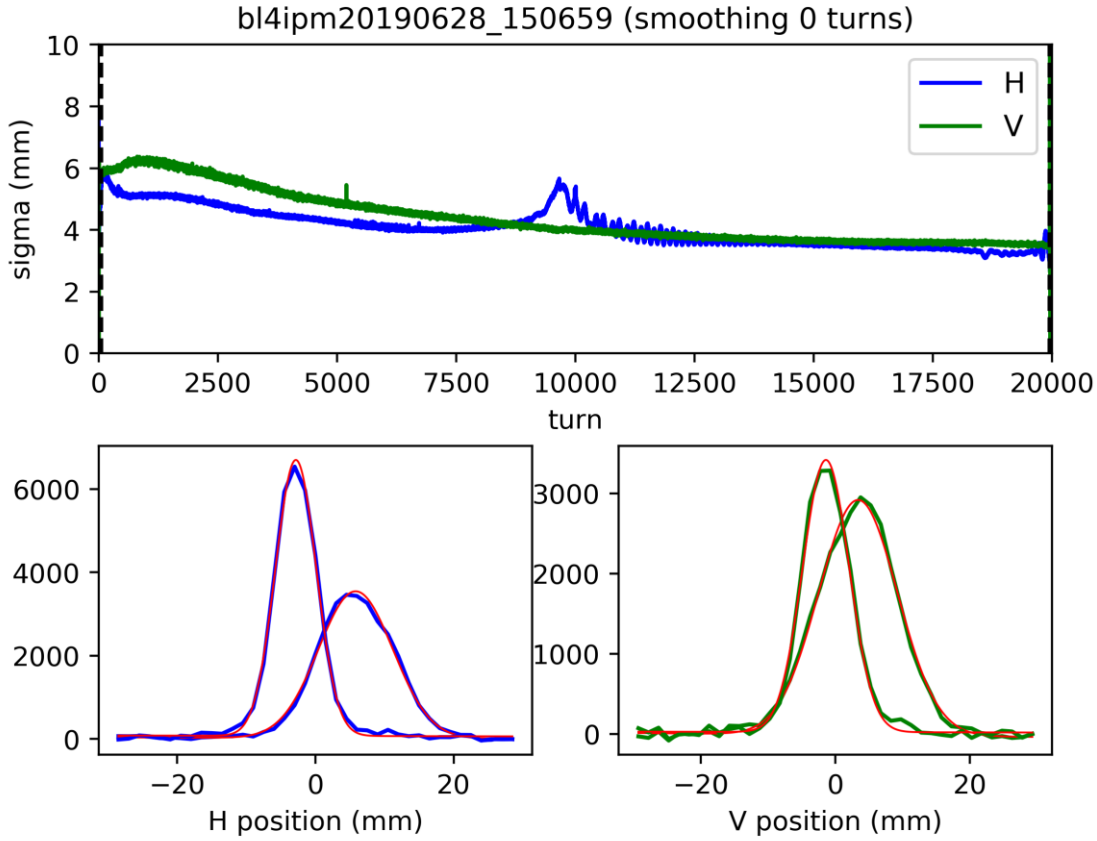

Figure 3: The IPM data over the Booster cycle with N_p=4.3·10^{12} and $Q_{x,y}$'=-4/-16: (top) the rms vertical and horizontal beam sizes; (bottom left) horizontal beam profiles measured at injection (broader peak) and extraction; (bottom right) same for the vertical IPM. Note, that slightly higher MCP voltage on the horizontal IPM of 650V (vs 600V in the vertical one) results in a stronger signal.

Theory of the IPM profile expansion is developed in [3], and the measured beam size σ_m is related to the original proton beam size σ_0 as:

$$\sigma_m = \sigma_0 h(N_p, \sigma_0, D, V, d) \quad , \quad (1)$$

where the factor h is

$$h\left(N_p, \sigma_0, D, V, d\right) \cong 1 + F\left(\frac{2U_{SC}\,D}{\sigma_0\,V}\right)\left[\frac{\Gamma(1/4)}{3}\left(\frac{d}{\sigma_0}\right)^{\frac{1}{2}} - \frac{\sqrt{\pi}}{2}\right] + \cdots, \qquad (2)$$

and V is the IPM extracting voltage (typically, 24 kV in our case) and D is its HV gap (103 mm), d is the distance for ions to travel from the beam orbit to the IPM collection plate, and the space-charge potential for the proton beam with current I is U_{SC} = 30[V]I/β_p. The numerical factor F is equal to 1 in the case of unbunched DC proton beam with Gaussian transverse current distribution while for uniform distribution with radius $a=2\sigma_0$, a similar analysis yields $F=2\sqrt{2}/\Gamma(1/4)\approx 0.78$, where gamma function $\Gamma(1/4)\approx 3.625$. In the case of Booster, with modest expansion $h<2$, one can neglect minor corrections due to somewhat unequal horizontal and vertical beam sizes, but should take into account the correction due to the bunch structure of the Booster current. The latter approximately scales as $(1+t_b/\tau_0)$ where t_b is the bunch spacing (some 19 ns at the end of the Booster cycle) and characteristic time for an ion to leave the beam $\tau_0=(2MD\sigma_0/ZeV)^{1/2}$, that is about 22 ns for typical IPM and beam parameters at the end of the cycle.

Also very important are intensity independent effects leading to the IPM profile smearing such as: a) the initial velocities of the ions; b) finite separation between the individual IPM charge collection strips; c) angular misalignment of the IPM long and narrow strips with respect to the high energy proton beam orbit; d) charging of dielectric material in between the strips or strip-to-stripe capacitive cross talk; e) non-uniformity of the extraction electric field in the operational IPM aperture. All these effects are monitor-specific and can be accounted via cross-calibration of low intensity beam sizes measured by the IPM $\sigma_{m,IPM}$ and by the MWs $\sigma_{m,MW}$. In that case, the rms instrumental smearing σ_T can be found via $\sigma^2_T = \sigma^2_{m,IPM}(N_p) - \sigma^2_{m,MW}(N_p)$, at $N_p \rightarrow 0$. Fig.4 a) shows that the rms IPM vertical beam sizes at extraction differ from the rms sizes measured by the MWs and recalculated to the IPM location, and that the difference grows with the total beam intensity.

Fig. 4 b) presents these differences $\sigma^2_{m,IPM}(N_p)$ - $\sigma^2_{m,MW}(N_p)$ for both vertical and horizontal beam size measurements with a zero-intensity intercept of $\sigma^2_T \approx 2.8 \pm 0.1$ mm^2.

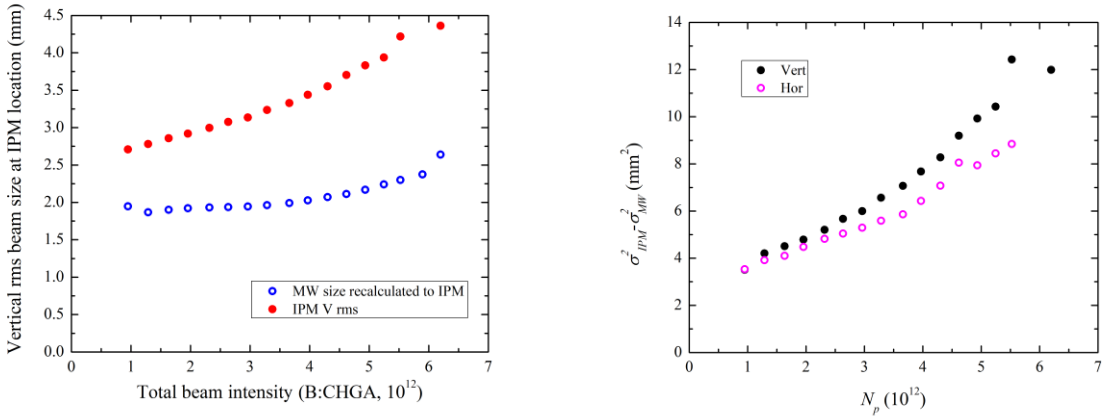

Figure 4: (left) Comparison of the rms IPM vertical beam sizes at extraction for different beam intensities with the rms sizes measured by the MWs and recalculated to the IPM location; (right) differences of vertical and horizontal IPM and MW mean squared beam sizes vs the total beam intensity.

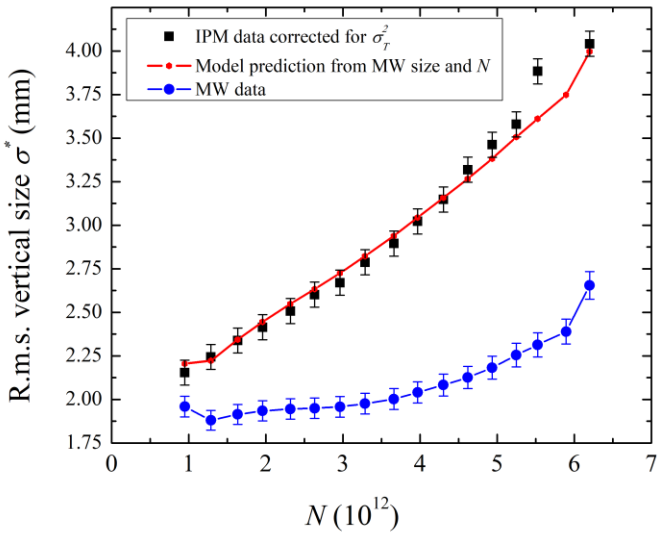

Figure 5: Vertical mean squared IPM size σ^* as measured at extraction (V=24 kV, D=103 mm, black squares) vs the total proton beam intensity N_p. The theoretical predication of Eq.(3) (with $d=D/2$=52 mm, red line) is calculated using the initial beam sizes σ_0 as measured by the Multi-Wires monitor (blue line). The measured IPM rms sizes $\sigma^2_{m,IPM}$ are corrected for the intensity independent smearing as $\sigma^* = (\sigma^2_{m,IPM}(N_p) - \sigma^2_T)^{1/2}$ with σ^2_T=2.7 mm^2.

Accounting for all the effects results in the expansion factor $h=(\sigma^2_{m,IPM}(N_p) - \sigma^2_T)^{1/2}/\sigma_0$ equal to:

$$h \cong 1 + 0.026\left(\frac{N_p}{10^{12}}\right)\left(\frac{D}{103\,\sigma_0}\right)\left(\frac{24\,kV}{V}\right)\left[\frac{\Gamma(1/4)}{3}\left(\frac{d}{\sigma_0}\right)^{\frac{1}{2}} - \frac{\sqrt{\pi}}{2}\right][1 + \frac{t_b}{\tau_0}], \qquad (3)$$

(see all details in Ref.[3]) that gives about 5% accuracy when applied to the Booster vertical IPM data – see Fig.5.

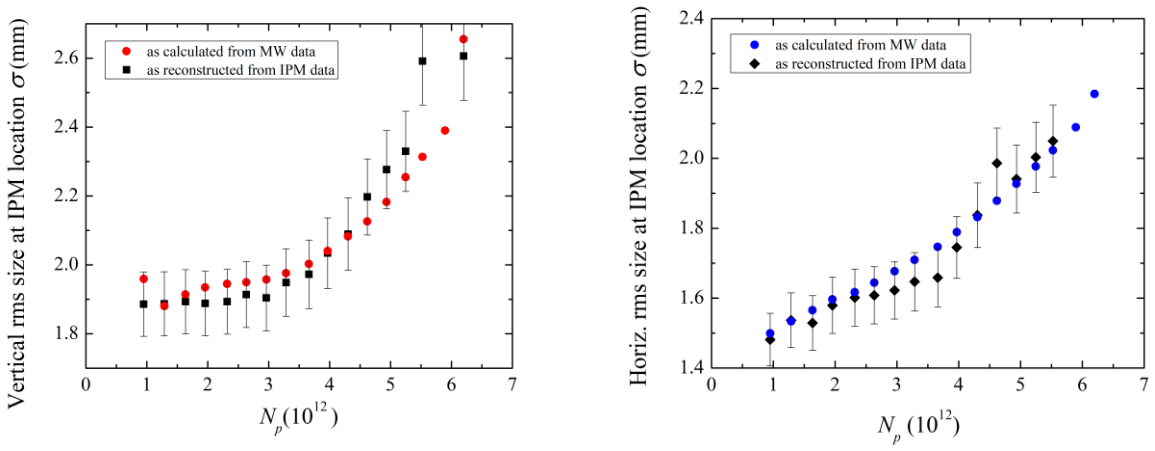

Figure 6: Comparisons of the vertical (left) and horizontal (right) rms beam sizes at extraction for a range of total proton beam intensities N_p. Red and blue dots are as measured by MWs and recalculated for the IPM location. Black squares with error bars are for the rms beam sizes reconstructed from the IPM data correction for σ^2_T and for the space-charge expansion $h(N_p, V, D, d)$ - see also in the text.

Knowing σ_T, N_p and the IPM voltage and gap V, D one can easily reverse Eq.(3) and find the original proton beam σ_0 from the measured and corrected $\sigma^* = (\sigma^2_{m,IPM}(N_p) - \sigma^2_T)^{1/2}$. There are many ways to find σ_0 from σ^*, i.e., to solve equations of the type of:

$$\sigma^* = \sigma_0\left(1 + \frac{c}{\sigma_0^{3/2}}\right), \qquad (4)$$

where c is a known constant – see Eq.(3). There is an exact solution of the cubic equation (4) that is close to $\sigma_0 \approx \sigma^*/(1+c/\sigma^{*3/2})$ at small c as but it is quite complicated and lengthy mathematical expression at moderate c. Note that for the highest intensity $N_p=6\cdot10^{12}$ the constant $c=2.53$ mm$^{3/2}$.

Slightly easier and straightforward is an iterative approximation. Analyzing the IPM data with modest expansion $h < 1+1/2^{1/3}$ we found even simpler practical algorithm that is good within 5% :

$$\sigma_0 \cong \frac{\sigma^*}{\left(1+\frac{c}{\sigma^{*\frac{3}{2}}}\right)\left(1+\alpha\frac{c^2}{\sigma^{*2}}\right)} \quad , \qquad (5)$$

where a fitting coefficient $\alpha \approx 0.42$ account for variety of higher order terms in Eqs.(3, 4). Figure 6 shows results of application of the above formula to the IPM data (corrected for σ_T) taken at the extraction and compared to the MW data. Fig.6 a) presents the comparison of the vertical rms beam size calculated from the MW emittance at extraction as $(\varepsilon_V\beta_V/\gamma)^{1/2}$. The agreement is good to about ±5% (error bars) over a wide range of the total proton intensities N_p. Similarly, the rms beam size derived from the horizontal IPM approximates well the horizontal rms beam size calculated from the MW emittance at extraction as $(\varepsilon_H\beta_H/\gamma+D^2_x(\Delta p/p)^2)^{1/2}$, where we used $\Delta p/p \approx (0.5\pm0.05\ N_p/10^{12})\cdot 10^{-3}$. In both cases we used $d=D/2=52$ mm, that might be only an approximation of a true distance from the beam orbit to the IPM's MCP plate. To get a better agreement in the horizontal plane approximately halved the additional intensity correction term in the denominator of Eq.(5) , i.e., used $\alpha \approx 0.21$.

Fig.7 illustrates the result of similar analysis for the evolution the measured IPM profiles of the Booster beam with $N_p=4.62\cdot10^{12}$. There, the red curve is for the rms vertical beam size $\sigma_{m,IPM}$ as measured by the IPM at each of 20 thousand turns of the Booster acceleration cycle; the black line represents the beam size after correction for the intensity independent smearing σ^*; and, finally, the true proton rms beam size σ_0 was reconstructed following the algorithm of Eqs. (1-3) and is represented by the blue line. One can see that the overall beam size correction is about 15% early in the Booster acceleration cycle when the rms beam size is about 6 mm. At the end of the cycle, with proton energy increased from 400 MeV to 8 GeV, the correction is almost by a factor of two and

accounting for the space-charge expansion is the most important. Also, one can see that the reconstructed IPM size at the end of the acceleration cycle matches well the extracted beam size measured by the Multi-Wires, as indicated by a black open circle with error bars at the left of Fig.7.

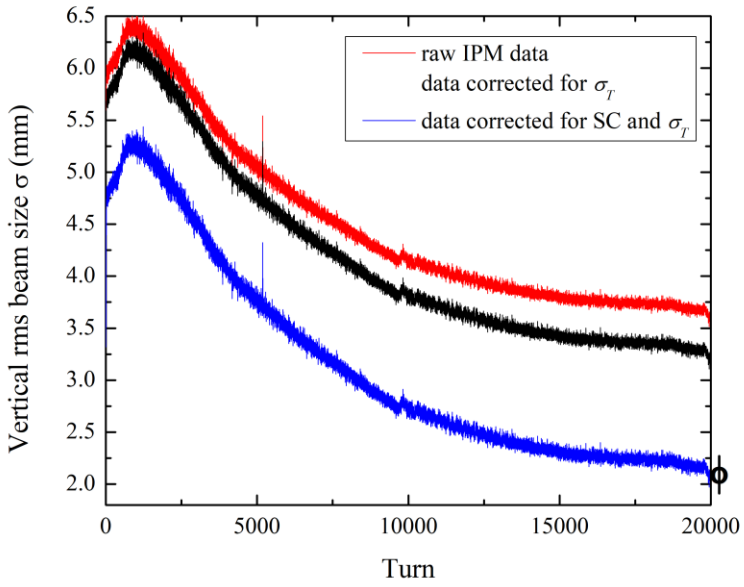

Figure 7: An example of reconstruction of vertical rms proton beam size in the 33 ms (20000 turns) acceleration cycle of the Fermilab 8 GeV Booster synchrotron with the total beam intensity of N_p=4.6·10^{12}: time dependence of the original IPM data (red), the data corrected for smearing effects (black) and the same data after additional correction for the space-charge expansion (blue) (from [3]).

2. BOOSTER BEAM EMITTANCE VS INTENSITY

The next natural step would be to apply the above analysis and calculated the evolution of the beam emittance over the Booster acceleration cycle from injection to extraction using the IPM data and Eq.(5) for the known N_p , σ_m and σ_T. Several important effects have to be carefully accounted for: (1) first of all, as indicated by Eq.(2), the space-charge expansion depends on the distance d from the beam orbit to the IPM collection plate. The proton beam orbit in the Booster is not stable, particularly in the horizontal plane, and varies by as much as some 16 mm along the

cycle – see Fig.8 - thus, affecting the vertical IPM profile expansion that scales with $d^{1/2}$; (2) Secondly, the beta-functions at the IPM locations vary in the cycle – see Fig.9 – as well as the space-charge forces which somewhat distort the optical focusing lattice functions; (3) last but not least, are the variations of the bunching factor and of the bunch spacing that affect the IPM profile expansion – see Eq.(3).

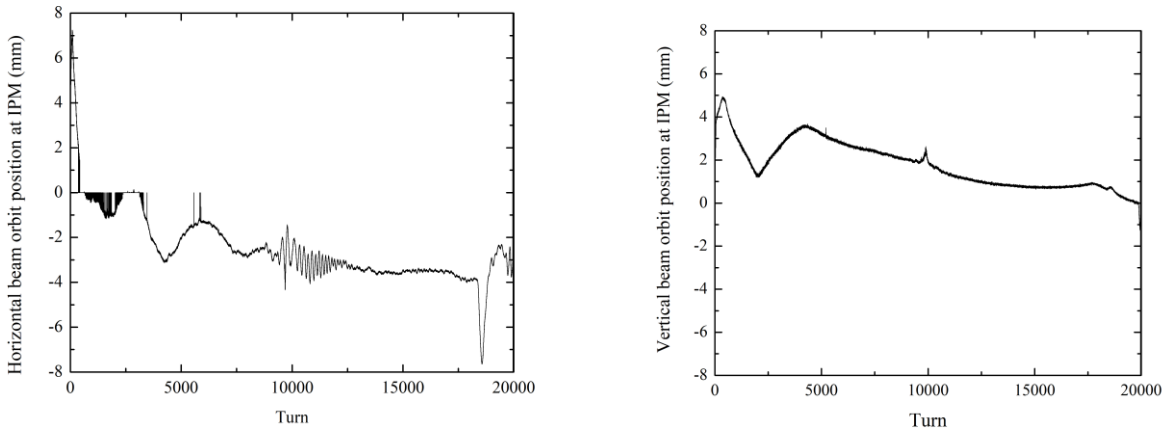

Figure 8: Horizontal (left) and vertical (right) proton beam orbit positions at the IPMs.

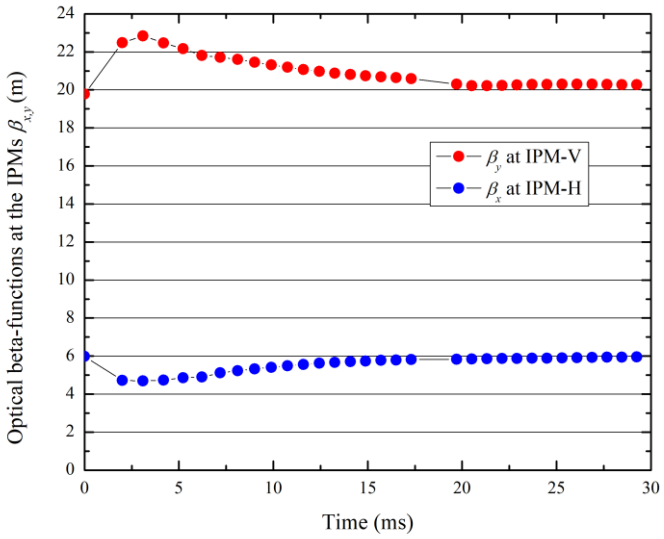

Figure 9: Horizontal and vertical beta-functions at the IPM locations during the Booster acceleration cycle, as calculated from known trim quadrupole currents.

Most of the above intensity independent effects can be accounted if one assumes no emittance growth at the lowest intensities. Various lines in Fig.10 illustrates how it can be done – starting with the IPM rms size (black line, raw data taken at N_p=0.5·10^{12}), one can calculate the rms normalized transverse emittance as $\varepsilon_V = \sigma^2_m \beta_V \beta_p \gamma_p$ (pink line, the beta-function at the IPM is about β_V=20.3 m). One can see that the emittance grows from some 1.5 mm mrad at injection to about 3 mm mrad right before extraction. Application of the intensity-independent correction $\sigma^* = (\sigma^2_{m,IPM}(N_p) - \sigma^2_T)^{1/2}$ with σ^2_T=2.8 mm^2 and the space-change expansion correction Eq.(5) results in the blue line that is flat within some 10-15% with some kind of parabolic variation along the cycle. That variation can be compensated by multiplier factor $G(t)=1/(1+0.14\cdot t/T + 0.018\cdot(1-T/2)^2/(T/2)^2)$ that is naturally equal to 1 at the end of the cycle $t=T$=33ms or 20000 turns : $G(T)$=1 – so, the calibration of the IPM wrt to the MW data at extraction is not affected. Brown line in Fig.1 is for the "double-corrected" emittance that is flat within about 5%.

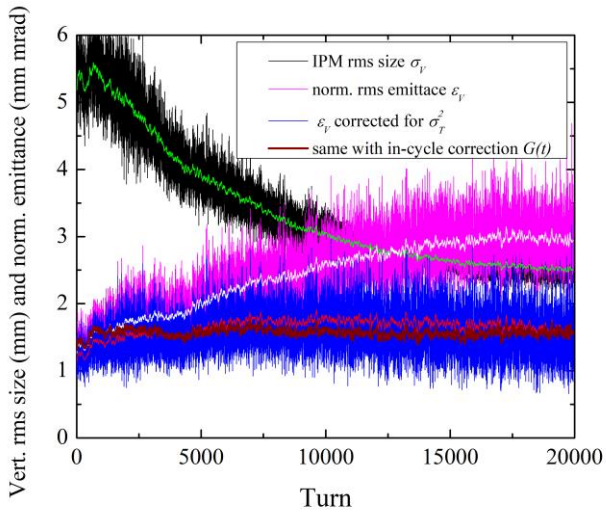

Figure 10: Vertical rms proton beam size and emittance at low intensity N_p=0.5·10^{12}: black – raw IPM data, green – 100 turn window average of the raw IPM data; pink and white – vertical rms normalized emittances calculated from the raw IPM data; blue and red – same, but corrected for intensity independent smearing; brown – same with additional fudge factor $G(t)$ – see text.

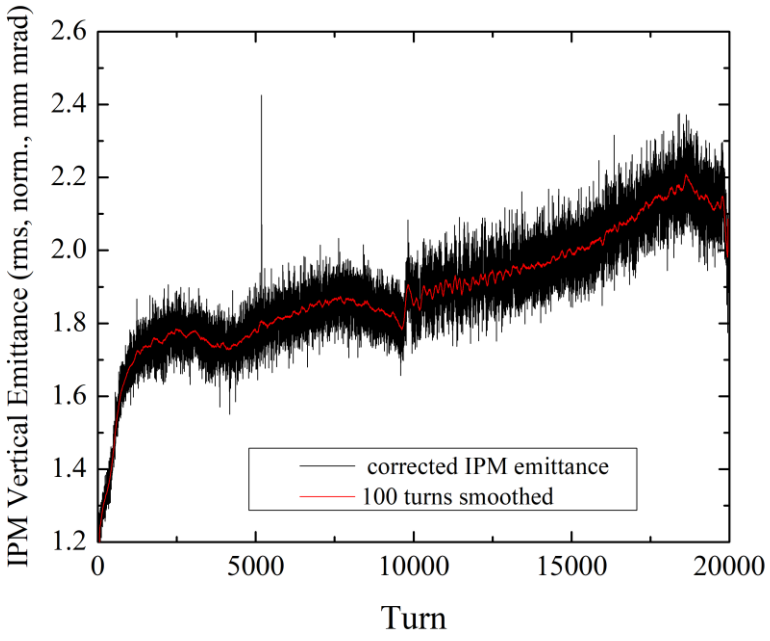

Figure 11: Vertical emittance at $N_p=4.6\cdot10^{12}$.

Results of the similar analysis for the operational intensity of $N_p=4.6\cdot10^{12}$ are shown in Fig.11. One can see the overall increase of the emittance from 1.2-1.3 mm mrad at injection to about 2.0-2.1 mm at extraction – that latter in a good agreement with the MW emittance data shown in Fig.2.

3. DISCUSSION: SPACE-CHARGE EFFECTS, SYSTEMATICS OF IPM SIGNALS, AND BOOSTER APERTURE

Above we have established proper IPM data correction algorithm, namely: a) subtract intensity-independent smearing and calculate $\sigma^* = (\sigma^2_{m,IPM}(N_p) - \sigma^2_T)^{1/2}$; b) then use the space-charge effect correction formulae Eq.(5) to find out σ_0 from σ^* and known N_p, V, D, d; c) then calculate the emittance taking the fudge factor G(t) into account $\varepsilon_V(t) = \sigma^2_0(t)\beta_V\beta_p(t)\gamma_p(t)G(t)$. Now, one can analyze the Booster emittance evolution for a wide range of intensities N_p from $0.5\cdot10^{12}$ (2 turns

injection) to $4.6 \cdot 10^{12}$ (20 turns) - see Fig.12. One can see that upto about $3.66 \cdot 10^{12}$ (12 turns, pink line)) the emittance is not growing much in the cycle and is about 1.4-1.6 mm mrad. Above that intensity the emittance evolution exhibits several features: i) fast growth over the first 2000-3000 turns - see also Fig. 13a, ii) steady growth for the rest of the cycle – see Fig.13 b; iii) spike at the time of transition – most probably related to the bunch shortening that amplifies the IPM space-charge profile expansion; and iv) some 5-10% variations at the end of the cycle which might be due to the horizontal orbit exclusion – see parameter d in Eq.(3) – and, at the very last hundreds of turns, bunch rotation in longitudinal phase-space prior the extraction in so that beam has a longer bunch length and a smaller momentum spread.

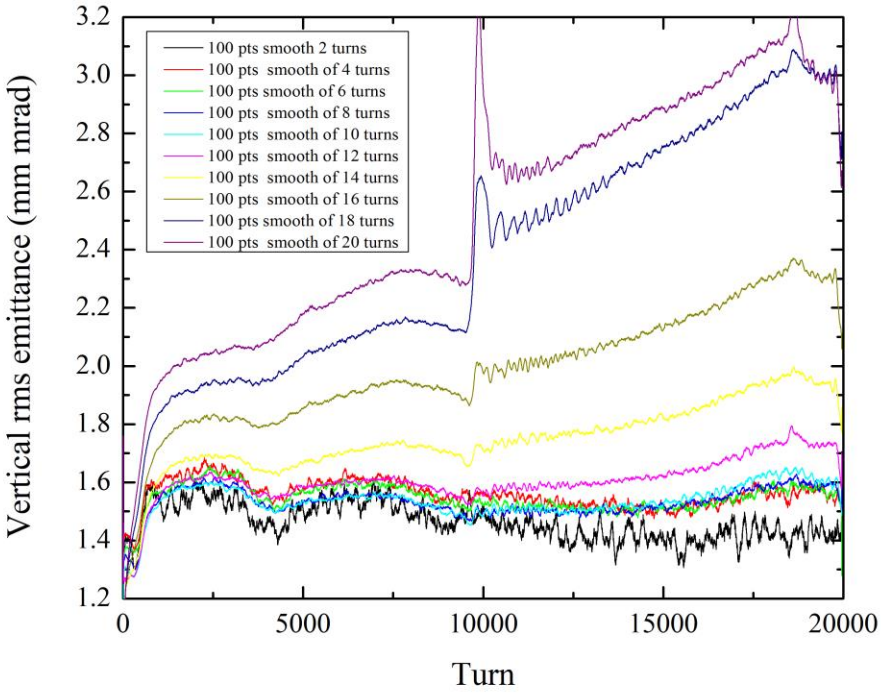

Figure 12: Evolution of the IPM vertical emittance (corrected) in the Booster cycle at different intensities N_p from $0.5 \cdot 10^{12}$ (2 turns injection) to $4.6 \cdot 10^{12}$ (20 turns injection).

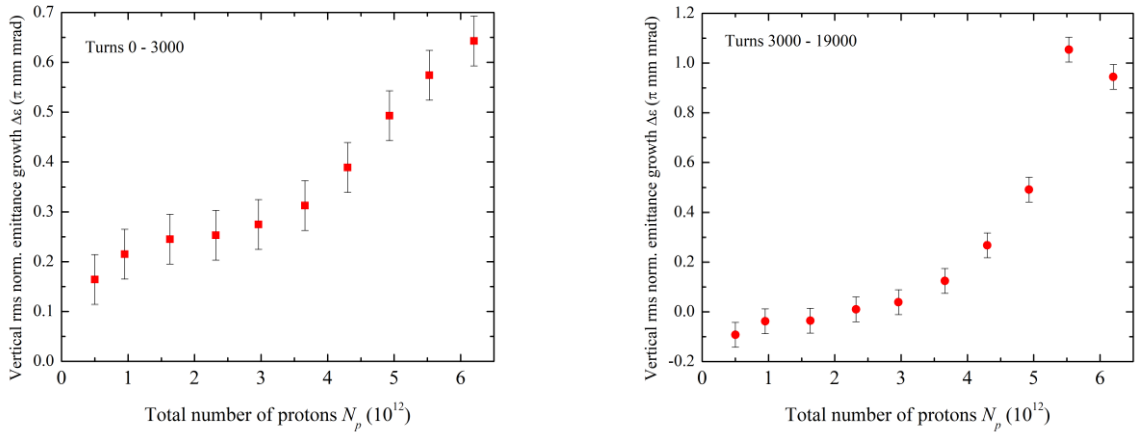

Figure 13: Vertical rms emittance growth vs N_p : (left) over the first 3000 turns; (right) from 3000 to 19000 turns. The data points are for the values averaged over five hundred turns 0-500, 3000-3500, 19000-19500. The error bars indicate estimated systematic uncertainty.

While the last two effects seem to be instrumental; the first one (fast growth early in the cycle) is probably due to proton space-charge effects. Indeed, at that time, the space-charge tuneshift parameter reaches very high value of about dQ_{SC}=0.7 - see Fig. 14. The reasons of the second effect – the slow emittance increase – are not very clear.

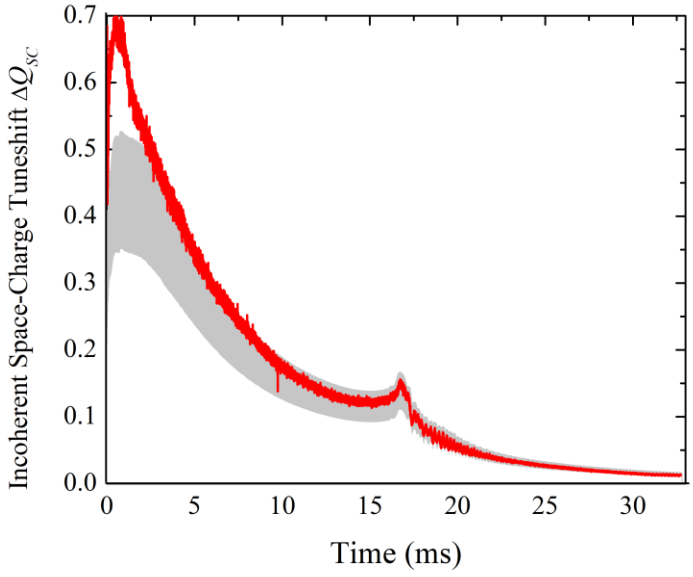

Figure 14: Calculated vertical space-charge tuneshift parameter for the Booster cycle with N_p=*4.6*·10^{12}.

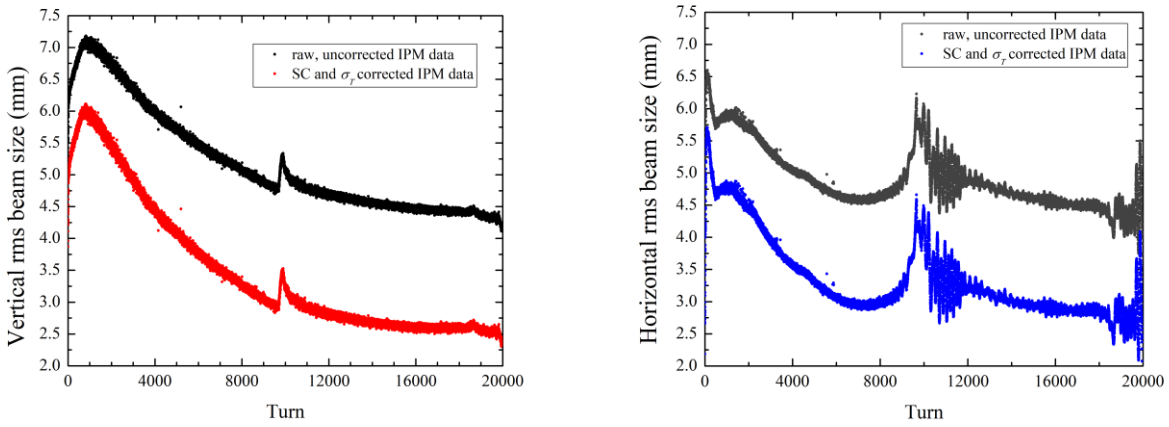

Figure 15: Vertical and horizontal rms IPM beam sizes' evolution over the Booster cycle at $N_p=6.2\cdot10^{12}$ (raw data – black line).

In our previous report [1] we identified two different types of the intensity related effects in the transmission of the Fermilab Booster: a) the losses that occur early in the cycle which scale approximately as a power of the SC tuneshift $\Delta N_p / N_p \sim dQ^{\kappa}_{SC}$ and b) the losses after the transition crossing which exhibit a threshold-like behavior above $6\cdot10^{12}$. Taking look at the dynamics of the corrected beam sizes measured by the IPMs , shown in Figs. 15a and 1b, one can conclude that the losses following the injection are most probably due to the vertical beam size expansion to some 6 mm, most probably caused by the space-charge effects. At the transition, the vertical beam size is small while the horizontal one, dominated by the dispersive contribution $D_x(\Delta P/P)$, becomes as large as 5 mm, and it is natural to assume that the proton losses at the transition end up at the horizontal aperture(s).

The Booster apertures have been extensively studied for the purpose of the operational optimization [4] as well as part of the Booster collimation system upgrade [5, 6]. Fig.16 depicts the

cross-sections of the Booster F and D combined-function magnets and indicates known aperture limitations. Table I below summarizes the beam sizes σ_y , σ_x (IPM data, corrected, at injection and transition, at nominal intensity $N_p=4.6\cdot10^{12}$ and $\Delta p/p=0.0017$ at injection and 0.0027 at transition), the physical apertures A_y , A_x in the absence of collimators, and their ratios for various locations around the ring including focusing and defocusing magnets, RF cavities and the IPMs.

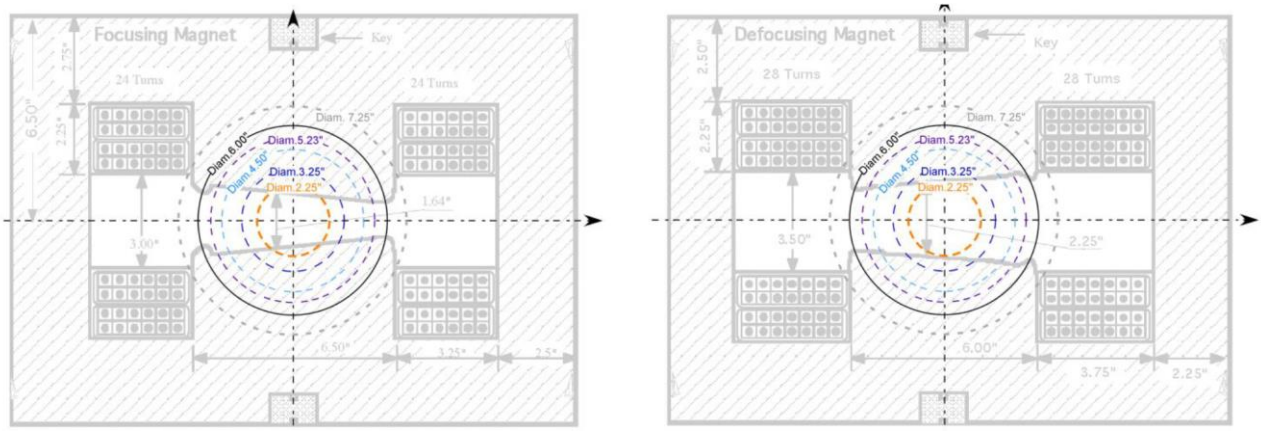

Figure 16: Cross Sectional View of a "F" magnet (left) and a "D" magnet [5] overlapped by apertures of some typical Booster elements implying possible aperture restrictions on the beam: a) RF-cavities (Diam. 2.25"); b) regular beam pipes (Diam. 3.25"); c) corrector package (Diam. 4.5"); d) special aperture in short straight 12 (Diam. 5.23" shifted horizontally by 2 cm outwards); e) 0.5 meter pipes between F and magnets (Diam. 6.00"); f) flanges of combined-function magnets (Diam. 7.25") – from Ref. [6].

Table I: Booster beam sizes and half-apertures without collimators.

element	β_y , β_x , D_x (m)	A_y / Ax (mm)	σ_y , σ_x (mm, inj.)	σ_y , σ_x (mm, tr.)	$(A/\sigma)_y$, $(A/\sigma)_x$ inj.	$(A/\sigma)_y$, $(A/\sigma)_x$ tr.
IPM	20.3 / 5.9 / 1.8	n/a	5.4 / 4.4	2.7 / 5.0	n/a	n/a
F magnet	10.8/33.8/3.2	21.8 / 54.6	3.9 / 8.8	2.0 / 8.6	5.6 / 6.2	11 / 6.3
D magnet	20.5/17.3/2.1	28.6 / 38.1	5.4 / 6.2	2.7 / 5.8	5.3 / 6.1	10.6 / 6.5
RF cavity	20.5 / 7.6 / 1.9	28.6 / 28.6	5.4 / 4.7	2.7 / 5.2	5.3 / 6.1	10.6 / 5.5

Table I summarizes the beam sizes σ_y, σ_x (IPM data, corrected, at injection and transition and nominal intensity $N_p=4.6\cdot10^{12}$) , the physical apertures A_y, A_x in the absence of collimators, and their ratios for various locations around the ring including focusing and defocusing magnets, RF cavities and the IPMs. One can see that the vertical A/σ ratio at injection as well the horizontal one at transition can be as small as 5.3-5.5. Orbit excursions of the order of 1-2 σ can further exacerbate the situation (see Figs.8a and 8b).

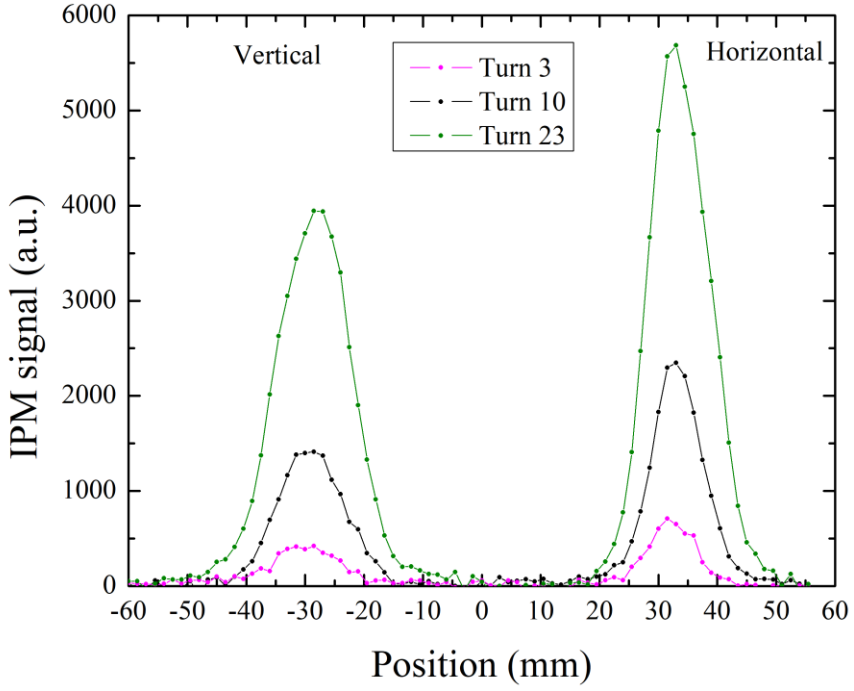

Figure 17: Vertical (left, positions from -60 to 0mm) and horizontal (right, from 0 to 60mm) IPM profiles as measured at the turns 3, 10, and 23 at $N_p=6.2\cdot10^{12}$ (uncorrected, raw IPM data).

The IPM data allow to take a close look into the dynamics of the beam profiles at the periods of significant particle intensity losses. Figs. 17 and 18 show the vertical (left half) and horizontal (right half) beam profiles measured at the turns 3, 10, 23, 50, 200 and 800 at the highest beam intensity we carried out studies with $N_p=6.2\cdot10^{12}$, which was characterized by the largest

losses of about 7% at injection. One can see a complex dynamics of the injection process itself (please, refer also to Table II): a) the beam intensity growing with every turn of the 20-turns injection process, accompanied by a small increase of the beams size $O(1\%)$ and orbit motion $O(1$ mm); b) that follows by several hundreds of turns (#50-#800) of the slowly declining intensity and relatively stable vertical orbit while and significant move of the horizontal orbit by some 5.5 mm without significant changes in the horizontal beam size. At the end of this process, the shape of the transverse distribution changes from a symmetric to a skewed one, most prominently in the vertical plane, where at the turn #800, the HWHM size asymmetry becomes as large as 1.5=10mm/6.5mm. That presents a clear indication of the losses - "shaving" of the beam halo on one side of the vertical aperture (and, possibly, to a smaller extent – on the horizontal aperture).

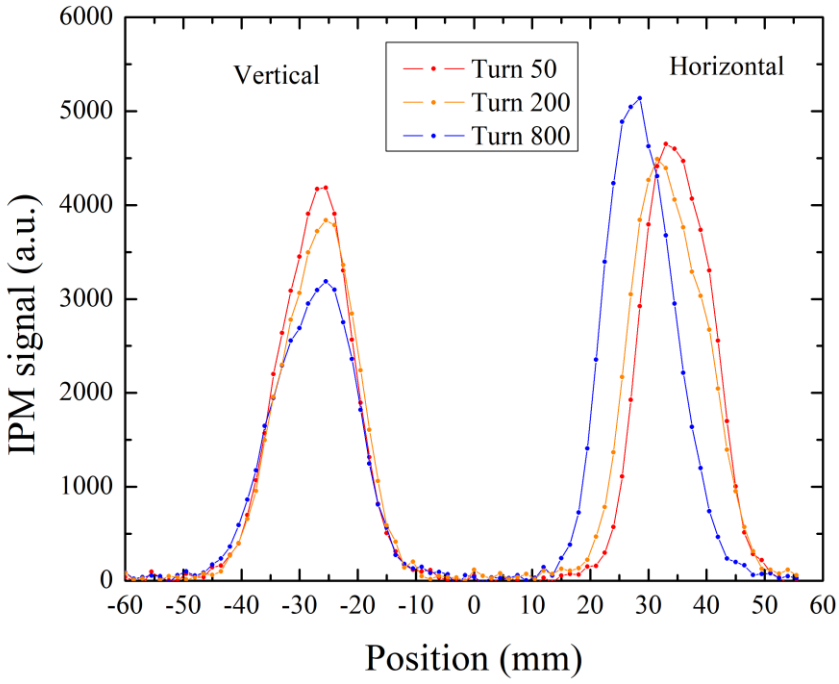

Figure 18: Vertical (left) and horizontal (right) IPM profiles as measured at the turns 50, 200, and 800 at $N_p=6.2\cdot10^{12}$.

Table II: Booster beam orbits *Y, X* (in mm) and intensities (relative to their values at the turn #23 at the end of the 20 turn injection), and rms sizes (in mm) at the different times of the acceleration cycle as measured by the IPMs in a cycle with the total intensity of $N_p=6.2\cdot10^{12}$. (Note that number of the turns injected is probably off by 1 or 2 from the reported turn number. Also, to note, that the IPM intensity, that is area under the curve in Figs.17,18, and 19b, is dependent on N_p and the ionization cross-section that, in turn, depends on the proton energy and type of residual gas molecules.

Turn #	Y	σ_y	N^*_y	X	σ_x	N^*_x
3	-1.4	5.6	0.09	-1.2	3.9	0.09
10	-0.5	5.5	0.32	-0.3	4.2	0.35
23	0	6.1	1	0	5.0	1
50	1.5	6.2	1.05	1.4	5.9	1.0
200	2.2	6.5	1.02	-0.2	6.5	1.03
800	3.0	7.0	0.91	-5.1	5.8	1.05
8000	0.1	5.0	0.81	-7.8	4.7	1.02
9664	-0.2	4.8	0.81	-8.3	6.1	1.15
12000	-1.1	4.7	0.78	-8.2	4.9	1.07

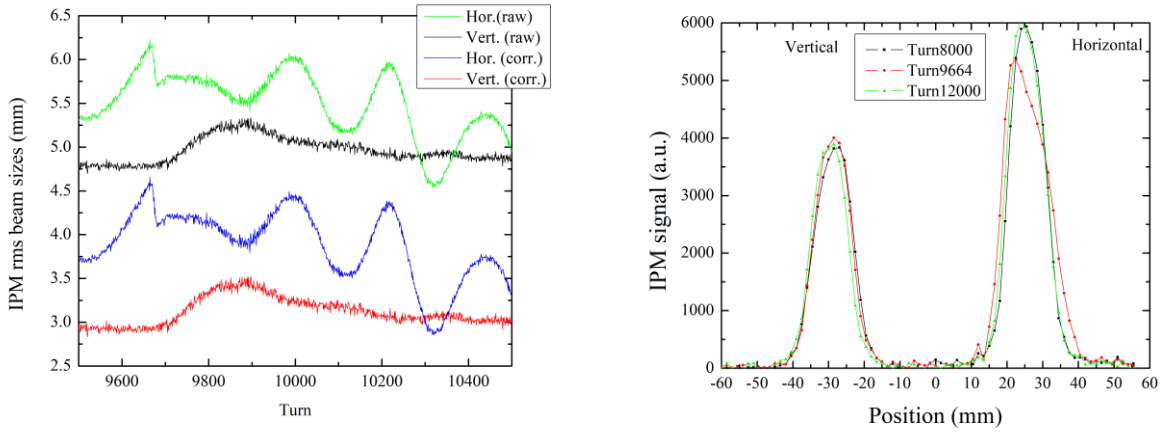

Figure 19: (left) detailed view of the dynamics of vertical and horizontal rms IPM beam sizes at transition at N_p=*6.2*·10^{12} (raw data and corrected data – compare with Fig.15); (right) vertical (left) and horizontal (right) IPM profiles as measured at the turns 8000, 9664, and 12000 at N_p=*6.2*·10^{12}(compare with Figs.16 and 17).

Of course, over the next hundreds and thousands of turns, the beam sizes are shrinking due to fast acceleration, the beam edges get away from the apertures and bema shape relax to more symmetric shapes. The shape asymmetry occurs again, and even stronger - at the transition – see Fig.19. It is most prominent in the horizontal profile on the turn #9664, when the ratio of the left and right HWHM are different by a factor of 3 – 3.5 mm and 10 mm, correspondingly. That is indicative of the beam losses *O*(7%) on a horizontal aperture at the transition. Note, that shortly before the transition (at the turn #8000) and shortly after it (#12000) the profiles are symmetric again.

4. DISCUSSION, CONCLUSIONS AND OUTLOOK

The above analysis indicates several key elements of the overall evolution of the beam emittance in the Booster. The injected Linac beam has the transverse emittance ε_0 *O*(0.7-1 π mm

mrad, rms normalized). In the process of multiturn injection, the beam goes multiple though the foil and via multiple scattering gets the emittance increase of :

$$\Delta\varepsilon_{foil} \cong (\beta\gamma)_p \frac{\beta_{x,y}}{2} \left(\frac{d}{X_0}\right)\left(\frac{13.6\ MeV}{pc}\right)^2 \times N_{turns}\ , \qquad (6)$$

that gives some 0.0077 π mm mrad per turn in the horizontal plane and 0.026 π mm mrad per turn in the vertical plane for the foil thickness d=380 μ gram/cm^2 , radiation length X_0=42 g/cm^2 and plane pc=953 MeV. The beam crosses the foil for approximately N_{BT}+18 turns [7], but it moves across and off the foil during the injection, so the effective number of turns is about N_{BT}+9 turns. Therefore, the estimated emittance increase at injection grows with the total circulating beam intensity (because the intensity scales with N_{BT}) and for the nominal N_{BT}=14 turns injection $\Delta\varepsilon_y$≈0.6π mm mrad and $\Delta\varepsilon_x$≈0.6π mm mrad. Over the next hundreds of turns the emittance grows due to the (intensity independent) decoherence injection error and quickly developing space-charge effects, so the additional increase at the turn 3000 is approximately (see Fig.12 and Fig.13a):

$$\Delta\varepsilon_{y,3000}\ [\pi\ \text{mm mrad}] \approx 0.2 + 0.41 \cdot (N_p/6\ 10^{12})^2 \qquad (7)$$

After that, the IPMs indicate further steady (~ t) increase – see Fig.12 and Fig.13 b:

$$\Delta\varepsilon_{y,3000\text{-}19000}\ [\pi\ \text{mm mrad}] \approx 0.97 \cdot (N_p/6\ 10^{12})^3 \qquad (8)$$

Finally, the emittance at extraction exhibits significant growth at high total beam intensities as (see Fig.2):

$$\Delta\varepsilon_{y,extr}\ [\pi\ \text{mm mrad}] \approx 1.7 + 1.20 \cdot (N_p/6\ 10^{12})^{4\pm0.3} \qquad (9)$$

$$\Delta\varepsilon_{x,extr}\ [\pi\ \text{mm mrad}] \approx 1.8 + 1.03 \cdot (N_p/6\ 10^{12})^{4\pm0.3} \qquad (9)$$

The intensity dependent emittance growth is strongly dependent on the chromaticity- see Fig.2 and Fig.20 a - and at the nominal intensity N_p= 4.5 10^{12} the emittance increases from about 2.1 π mm

mrad to some 2.4 π mm mrad (vertical) and 2.7 π mm mrad if the operational chromaticity at at the first ms after the injections is changed from $Q'_{x,y}$=-4/-16 to -20/-20.

We also found out that the increase of the space-charge induced losses after injection is taken place together with the emittance growth and results in asymmetric vertical beam profiles. Similarly, the horizontal beam shape asymmetry appears at when a high intensity beam traverses the transition energy.

The Booster Ionization Profile Monitors operate in the ion collection mode without external magnetic field and extremely valuable tools for fast beam size diagnostics. There are strong systematic space-charge effects in the IPMs leading to significant, factor of 2 or more, expansion of the rms beam size reported by the IPMs w.r.t. to the original proton beam size. We accounted these effects following theoretical recipes Ref.[3]. Some subtle effects, e.g. those due to variable bunching factor need further exploration and experimental studies. In general, the theoretical analysis must be augmented and confirmed by future experimental beam studies. On January 28, 2020, we have attempted a short one to study the effect of the IPM voltage V on the measured profiles – see Fig.20 b – and observed the size reduction vs V. Note, that the differential IPM profile measurements and several values of V may allow to estimate the actual proton beam size σ_0 as approximation for V going to infinity using Eq.(2).

Of note, the IPM signals, if taken at very high time resolution of better than 10 ns, could allow quantitative analysis of the Booster vacuum composition , as the arrival times (from the beam to the MCP plate) depends on the ion species $\tau_0=(2MD\sigma_0/ZeV)^{1/2}$ – see also Ref.[3].

Experimental studies of the Booster losses and emittance evolution are of great importance to predict the machine operational conditions in the PIP-II era and have to be continued.

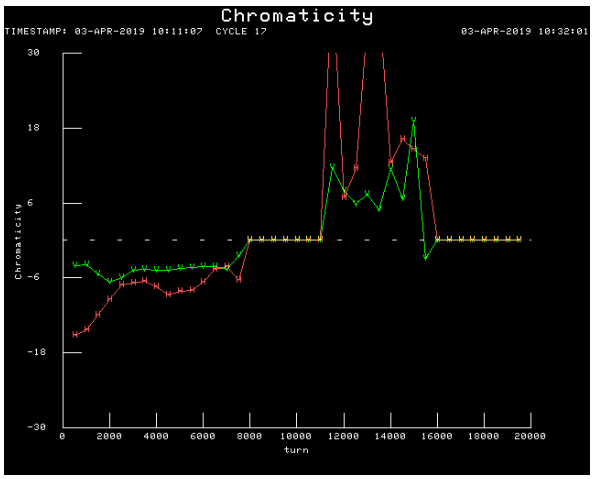

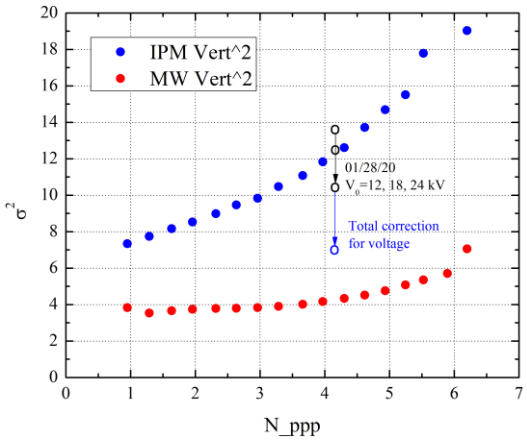

Figure 20: (left) vertical(red) and horizontal (green) machine chromaticities $Q'_{x,y}$ in the nominal (operational) Booster cycle; (right) initial study of the IPM voltage effect on 01/28/2020 – empty points are for the vertical mean squared beam size as reported by the Booster IPM with voltages V=12, 18 and 24 kV at nominal $N_p=4.5\cdot10^{12}$, red and blue dots – MW and IPM data at V=24 kV taken in the Summer 2019 studies (see text).

ACKNOWLEDGEMENTS

We would like to thank C.Y. Tan, C. Bhat, Yu. Alexahin, A. Burov, S. Nagaitsev, W. Pellico and R. Thurman-Keup for numerous discussions on the topics of this study and S. Chaurize, V. Kapin and K. Triplett for their invaluable help with experimental Booster beam studies. In addition, the Summer 2019 Booster beam study campaign involved N. Eddy, C. Jensen, J. Larson, and H. Pfeffer of Fermilab, H. Bartosik, N. Biancacci, M. Carla, A. Saa Hernandez, A. Huschauer, F. Schmidt of CERN, D. Bruhwiler, J. Edelen of the Radiasoft SBIR company and V. Kornilov of GSI. We greatly appreciate their fruitful cooperation and the spirit of international beam physics collaboration.

Fermilab is supported by U.S. Department of Energy, Office of Science, Office of High Energy Physics, under Contract No. DE-AC02-07CH11359.

REFERENCES

[1] V.Shiltsev, J.Eldred, V.Lebedev, K.Seiya, Studies of Beam Intensity Effects in Fermilab Booster Synchrotron. Part I: Introduction; Tune and Chromaticity Scans of Beam Losses", Fermilab Preprint FN-2020-2740 (2020).

[2] J.Eldred, Physics Studies for High Intensity Proton Beams at the Fermilab Booster, in Proc. NAPAC2019 (Lansing, MI, USA, Sep.1-6, 2019), WEPLO10; Fermilab Beams-Doc-7610 (https://beamdocs.fnal.gov/).

[3] V.Shiltsev, Beam Size Reconstruction from Ionization Profile Monitors, arXiv:2003.09072 (2020)

[4] K.Seyia, et al., arXiv: 1301.7350

[5] V. Kapin, Fermilab *beams-doc-5519* (2017), unpublished.

[6] V. Kapin, Fermilab *beams-doc-8457* (2020), unpublished.

[7] J.Eldred, C. M. Bhat, S. Chaurize, V. Lebedev, S. Nagaitsev, K. Seiya, C. Y. Tan, R. J. Tesarek, Foil Scattering Model for Fermilab Booster, arXiv:1912.02896